

$S = -1$ Meson-Baryon Unitarized Coupled Channel Chiral Perturbation Theory and the $S_{01} - \Lambda(1405)$ and $-\Lambda(1670)$ Resonances

C. García-Recio*, J. Nieves†, E. Ruiz Arriola,‡

Departamento de Física Moderna, Universidad de Granada, E-18071 Granada, Spain

M. J. Vicente Vacas

Dpto. Física Teórica and IFIC, Centro mixto Universidad de Valencia-CSIC,

Aptd. 22085, E-46071 Valencia, Spain

June 19, 2019

Abstract

The s -wave meson-baryon scattering is analyzed for the strangeness $S = -1$ and isospin $I = 0$ sector in a Bethe-Salpeter coupled channel formalism incorporating Chiral Symmetry. Four channels have been considered: $\pi\Sigma$, $\bar{K}N$, $\eta\Lambda$ and $K\Xi$. The required input to solve the Bethe-Salpeter equation is taken from lowest order Chiral Perturbation Theory in a relativistic formalism. There appear undetermined low energy constants, as a consequence of the renormalization of the amplitudes, which are obtained from fits to the $\pi\Sigma \rightarrow \pi\Sigma$ mass-spectrum, to the elastic $\bar{K}N \rightarrow \bar{K}N$ and $\bar{K}N \rightarrow \pi\Sigma$ t -matrices and to the $K^-p \rightarrow \eta\Lambda$ cross section data. The position and residues of the complex poles in the second Riemann Sheet of the scattering amplitude determine masses, widths and branching ratios of the $S_{01} - \Lambda(1405)$ and $-\Lambda(1670)$ resonances, in reasonable agreement with experiment. A good overall description of data, from $\pi\Sigma$ threshold up to 1.75 GeV, is achieved despite the fact that three-body channels have not been explicitly included.

PACS: 11.10.St; 11.30.Rd; 11.80.Et; 13.75.Lb; 14.40.Cs; 14.40.Aq

Keywords: Chiral Perturbation Theory, Unitarity, $\pi\Sigma$ -Scattering, $\bar{K}N$ -Scattering, $\eta\Lambda$ -Scattering, $S_{01} - \Lambda$ Resonances, Coupled channels, Bethe-Salpeter Equation.

*email:g_recio@ugr.es

†email:jmnieves@ugr.es

‡email:earriola@ugr.es

1 Introduction

Baryon resonances are outstanding features in elastic and inelastic meson-baryon scattering and signal the onset of non-perturbative physics. Constituent quark model approaches describe them as excited baryonic bound states, and the coupling to the continuum is obtained by evaluating transition matrix elements [1] but comparison with data can only be done once the scattering problem is solved. In such a scheme, the underlying quark constituent nature of hadrons is taken into account but implementation of Chiral Symmetry (CS) becomes difficult. In the region of low energies, it seems appropriate to start considering the hadrons as the relevant degrees of freedom where CS not only proves helpful to restrict the type of interactions between mesons and baryons, but also provides an indirect link to the underlying Quantum Chromo Dynamics (QCD) [2]. For processes involving Baryons and Mesons, Heavy Baryon Chiral Perturbation Theory (HBChPT) [3, 4] incorporates CS at low energies in a systematic way, and has provided a satisfactory description of πN scattering in the region around threshold [5, 6, 7]. It suffers, however, from known limitations. Firstly, the expansion is manifestly not relativistically invariant, and some convergence problems have been pointed out and solved by defining a proper regularization scheme [8]. The new scheme has successfully been applied to πN elastic scattering [9]. Secondly, the approach is based on a perturbative expansion of a finite amount of Feynman diagrams, it needs to be supplemented by some non-perturbative resummation to accommodate resonances. Regarding the second limitation, several unitarization methods have been suggested in the literature and previously used to describe the meson-baryon dynamics: Inverse Amplitude Method (IAM) [10], or a somehow modified IAM to account for the large baryon masses [11], dispersion relations [12, 13], Lippmann-Schwinger Equation (LSE) and Bethe-Salpeter Equation (BSE) [14, 15, 16, 17, 18, 19, 20, 23, 24].

In this work, we will study the s -wave meson-baryon scattering for the strangeness $S = -1$ and isospin $I = 0$ sector in a Bethe-Salpeter coupled channel formalism incorporating CS. This reaction provides a good example of the need of unitarization methods. The recent work of Ref. [25] shows that HBChPT to one loop fails completely already at threshold. The $\bar{K}N$ scattering length turns out to have a real part about the same size but with opposite sign and half the imaginary expected experimentally [26], due to the nearby subthreshold $\Lambda(1405)$ -resonance. The first study of the strangeness $S = -1$ and isospin $I = 0$ meson-baryon channel incorporating CS and unitarization was carried out in Ref. [15], though some phenomenological form factors were employed. More recently, this channel has been studied in Refs. [17] and [18], where a three-momentum cut-off is used to renormalize the LSE and the off-shell behavior is partially taken into account. In principle, this minimal renormalization procedure is acceptable but may turn out to be too restrictive in practice. If, instead, one takes advantage of the flexibility allowed by the renormalization of an Effective Field Theory (EFT), there is a chance of improving the description from threshold up to the resonance region and above. In practical terms this means increasing the number of counter terms which one has to add to make finite the amplitudes. Of course, there exist relations between these counter terms, as demanded by crossing symmetry and CS constraints, but, by neglecting the off-shellness of the LSE kernel and using a momentum cut-off to regularize the LSE, one introduces new constraints. This point was discussed at length in Ref. [27] in the context of elastic $\pi\pi$ scattering; from there one easily realizes that the renormalization scheme pursued in Ref. [17] would lead to a scenario where only one of the four $SU(2)$ -Gasser-Leutwyler $\bar{l}_1, \bar{l}_2, \bar{l}_3$ and \bar{l}_4 parameters is independent. This is the reason why, despite of the great success of the model of Ref. [17] in describing the data around the antikaon-nucleon threshold, including the features of the $S_{01} - \Lambda(1405)$ resonance, its predictions for higher energies [18] do not work so

well and clear discrepancies with data appear. Indeed, the limitations of the model of Ref. [17] did already appear in the strangeness $S = 0$ and isospin $I = 1/2$ meson-baryon sector, where the model is able to describe data only in a more or less narrow energy window around the $N(1535)$ resonance [19, 20]. However, the model previously developed by two of us for the latter channel in Ref. [23] describes data in a wider energy region, ranging from πN threshold up to almost a Center of Mass (CM) meson-baryon energy of $\sqrt{s} = 2$ GeV, including the features of a second resonance ($N(1650)$). Motivated by these encouraging results we extend in this work the model of Ref. [23] to the strangeness $S = -1$ and isospin $I = 0$ meson-baryon channel. Like in the $S = 0$ sector, taking into account the off-shellness of the BSE generates a rich structure of unknown constants which allow for a better description of the amplitudes. Although the generation of more undetermined constants may appear a less predictive approach than putting a cut-off (one single parameter) to regularize the divergent integrals, it reflects the real state of the art of our lack of knowledge on the underlying QCD dynamics. The number of adjustable Low Energy Constants (LEC's) should not be smaller than those allowed by the symmetry; this is the only way both to falsify all possible theories embodying the same symmetry principles and to widen the energy interval which is being described. Limiting such a rich structure allowed by CS results in a poor description of experimental data. However, a possible redundancy of parameters is obviously undesirable. The number of LEC's is controlled to any order of the calculation by crossing symmetry. In a unitarized approach, the only way to avoid this parameter redundancy is to match the unitarized amplitude to one obtained from a Lagrangian formalism¹. There is no standard one loop ChPT calculation for the meson-baryon reaction with open channels to compare with. Some results there exist within the HBChPT scheme, up to order $\mathcal{O}(1/M^3 f_\pi^2, 1/M f_\pi^4)$ – being M a typical baryon mass – but only involving pions and nucleons [7]. An indirect way to detect such a parameter redundancy might be through a fit to experimental data if the errors and correlations in some parameters turn out to be very large. We will adopt this point of view in this work, and will show that indeed correlations take place effectively reducing the total number of independent parameters.

In this paper four coupled channels have been considered: $\pi\Sigma$, $\bar{K}N$, $\eta\Lambda$ and $K\Xi$ and taken into account $SU(3)$ –breaking symmetry effects but neglected the considerably smaller isospin violation ones. Preliminary results of the present work can be found in [21, 22].

The paper is organized as follows: In Sect. 2, a summary of the theoretical framework used is described. Further details can be found in Ref. [23]. Numerical results for amplitudes and cross sections and details of the fitting procedure are given in Sect. 3. A special attention is paid both to the analytical properties, in the complex plane, of the found t matrix and to the statistical correlations between the fitted LEC's, being the Appendices A and B devoted to these issues as well. Finally, in Sect.4 we outline the conclusions of our work.

2 Theoretical framework

The coupled channel scattering amplitude for the baryon-meson process in the isospin channel $I = 0$

$$B(M_A, P - k, s_A) + M(m_A, k) \rightarrow B(M_B, P - k', s_B) + M(m_B, k') \quad (1)$$

with baryon (meson) masses M_A and M_B (m_A and m_B) and spin indices (helicity, covariant spin, etc...) s_A, s_B , is given by

$$T_P[B\{k', s_B\} \leftarrow A\{k, s_A\}] = \bar{u}_B(P - k', s_B) t_P(k, k') u_A(P - k, s_A) \quad (2)$$

¹See discussion in Appendix D of Ref. [23]

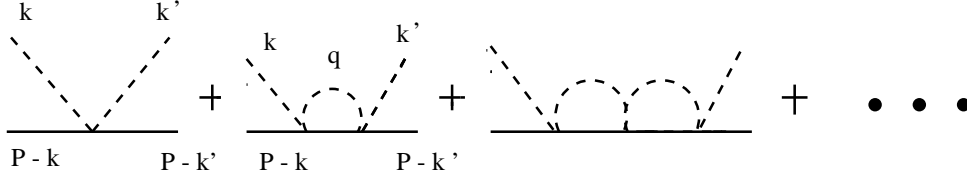


Figure 1: Diagrams summed by the Bethe Salpeter equation. Kinematics defined in the main text.

Here, $u_A(P - k, s_A)$ and $u_B(P - k', s_B)$ are baryon Dirac spinors² for the ingoing and outgoing baryons respectively, P is the conserved total four momentum and $t_P(k, k')$ is a matrix in the Dirac and coupled channel spaces. On the mass shell the parity and Lorentz invariant amplitude t_P can be written as:

$$t_P(k, k')|_{\text{on-shell}} = t_1(s, t)\not{P} + t_2(s, t) \quad (3)$$

with $s = P^2 = \not{P}^2$, $t = (k - k')^2$ and t_1 and t_2 matrices in the coupled channel space.

In terms of the matrices t_1 and t_2 defined in Eq. (3), the s -wave coupled-channel matrix, $f_0^{\frac{1}{2}}(s) [f_L^J]$, is given by:

$$\left[f_0^{\frac{1}{2}}(s) \right]_{B \leftarrow A} = -\frac{1}{8\pi\sqrt{s}} \sqrt{\frac{|\vec{k}_B|}{|\vec{k}_A|}} \sqrt{E_B + M_B} \sqrt{E_A + M_A} \left[\frac{1}{2} \int_{-1}^1 d\cos\theta \left(\sqrt{s} t_1(s, t) + t_2(s, t) \right) \right]_{BA} \quad (4)$$

where the CM three-momentum moduli read

$$|\vec{k}_i| = \frac{\lambda^{\frac{1}{2}}(s, M_i^2, m_i^2)}{2\sqrt{s}} \quad i = A, B \quad (5)$$

with $\lambda(x, y, z) = x^2 + y^2 + z^2 - 2xy - 2xz - 2yz$ and $E_{A,B}$ the baryon CM energies. The phase of the matrix T_P is such that the relation between the diagonal elements ($A = B$) in the coupled channel space of $f_0^{\frac{1}{2}}(s)$ and the inelasticities (η) and phase-shifts (δ) is the usual one,

$$\left[f_0^{\frac{1}{2}}(s) \right]_{AA} = \frac{1}{2i|\vec{k}_A|} \left(\eta_A(s) e^{2i\delta_A(s)} - 1 \right) \quad (6)$$

Further details on normalizations and definitions of the amplitudes can be seen in Section IIB of Ref. [23].

To compute the amplitude t_P we solve the BSE (see Fig. (1))

$$t_P(k, k') = v_P(k, k') + i \int \frac{d^4q}{(2\pi)^4} t_P(q, k') \Delta(q) S(P - q) v_P(k, q) \quad (7)$$

where $t_P(k, k')$ is the scattering amplitude defined in Eq. (2), $v_P(k, k')$ the two particle irreducible Green's function (or *potential*), and $S(P - q)$ and $\Delta(q)$ the baryon and meson exact propagators respectively. The above equation turns out to be a matrix one, both in the coupled channel and Dirac spaces. For any choice of the *potential* $v_P(k, k')$, the resulting scattering amplitude $t_P(k, k')$

²We use the normalization $\bar{u}u = 2M$.

fulfills the coupled channel unitarity condition, discussed in Eq. (21) of Ref. [23]. The BSE requires some input potential and baryon and meson propagators to be solved. To compute the lowest order of the BSE-based expansion [27] is enough to approximate the iterated *potential* by the chiral expansion lowest order meson-baryon amplitudes in the desired strangeness and isospin channel, and the intermediate particle propagators by the free ones (which are diagonal in the coupled channel space). From the meson-baryon chiral Lagrangian [2] (see Sect. IIA of Ref. [23]), one gets at lowest order for the *potential*:

$$v_P(k, k') = t_P^{(1)}(k, k') = \frac{D}{f^2}(\not{k} + \not{k}') \quad (8)$$

with D the coupled-channel matrix,

$$D_{S=-1}^{I=0} = \frac{1}{4} \begin{pmatrix} \bar{K}N & \pi\Sigma & \eta\Lambda & K\Xi \\ -3 & \sqrt{3/2} & -3/\sqrt{2} & 0 \\ \sqrt{3/2} & -4 & 0 & -\sqrt{3/2} \\ -3/\sqrt{2} & 0 & 0 & 3/\sqrt{2} \\ 0 & -\sqrt{3/2} & +3/\sqrt{2} & -3 \end{pmatrix} \begin{matrix} \bar{K}N \\ \pi\Sigma \\ \eta\Lambda \\ K\Xi \end{matrix} \quad (9)$$

given in the isospin basis and the same phase conventions as in Ref. [23].

While amplitudes follow the chiral symmetry breaking pattern from the effective Lagrangian to a good approximation, it is well known that physical mass splittings have an important influence when calculating the reaction phase space. Indeed, the correct location of reaction thresholds requires taking physical masses for the corresponding reaction channels. We have taken into account this effect in our numerical calculation. We also incorporate explicit CS effects to the weak meson decay constants and different numerical values for f_π , f_K and f_η can be used. This can be easily accomplished through the prescription

$$D/f^2 \rightarrow \hat{f}^{-1} D \hat{f}^{-1} \quad , \quad \hat{f} \equiv \text{Diag}(f_K, f_\pi, f_\eta, f_K) \quad (10)$$

The solution of the BSE with the kernel specified above can be found in Ref. [23]. It turns out that the functions t_1 and t_2 , defined in Eq. (3), do not depend on the Mandelstam variable t , and thus the dynamics is governed by the matrix function $t(s)$ (see Eq. (4))

$$t(s) = \sqrt{s} \, t_1(s) + t_2(s), \quad (11)$$

which is given in Eq. (34) of Ref. [23]. There, the renormalization of the obtained amplitudes is studied at length. As a result of the renormalization procedure, and besides the physical and weak meson decay constants, a total amount of 12

$$\begin{matrix} J_{\bar{K}N}, & J_{\pi\Sigma}, & J_{\eta\Lambda}, & J_{K\Xi} \\ \Delta_N, & \Delta_\Sigma, & \Delta_\Lambda, & \Delta_\Xi, \\ \Delta_{\bar{K}}, & \Delta_\pi, & \Delta_\eta, & \Delta_K \end{matrix} \quad (12)$$

undetermined LEC's appear. We fit these constants to data, as we will see in the next section, and from them we define the three following diagonal matrices:

$$\begin{aligned}
J_0(s = (\hat{m} + \hat{M})^2) &= \begin{pmatrix} J_{\bar{K}N} & 0 & 0 & 0 \\ 0 & J_{\pi\Sigma} & 0 & 0 \\ 0 & 0 & J_{\eta\Lambda} & 0 \\ 0 & 0 & 0 & J_{K\Xi} \end{pmatrix} \\
\Delta_{\hat{M}} &= \begin{pmatrix} \Delta_N & 0 & 0 & 0 \\ 0 & \Delta_\Sigma & 0 & 0 \\ 0 & 0 & \Delta_\Lambda & 0 \\ 0 & 0 & 0 & \Delta_\Xi \end{pmatrix} \\
\Delta_{\hat{m}} &= \begin{pmatrix} \Delta_{\bar{K}} & 0 & 0 & 0 \\ 0 & \Delta_\pi & 0 & 0 \\ 0 & 0 & \Delta_\eta & 0 \\ 0 & 0 & 0 & \Delta_K \end{pmatrix}
\end{aligned} \tag{13}$$

which appears in the solution of the BSE. We have denoted the meson-baryon low energy constants $J_0(s = (m_i + M_j)^2)$, $i = \bar{K}, \pi, \eta, K$ and $j = N, \Sigma, \Lambda, \Xi$ of Eq. (A8) of Ref. [23] as J_{ij} .

3 Numerical results

Throughout the paper we will use the following numerical values for masses and weak decay constants of the pseudoscalar mesons (all in MeV),

$$\begin{aligned}
m_K = m_{\bar{K}} &= 493.68 & m_\pi &= 139.57 & m_\eta &= 547.3 \\
M_p &= 938.27 & M_\Sigma &= 1189.37 & M_\Lambda &= 1115.68 & M_\Xi &= 1318.0 \\
f_\pi = f_\eta = f_K &= 1.15 \times 93.0
\end{aligned} \tag{14}$$

where for the weak meson decay constants we take for all channels an averaged value.

3.1 Fitting procedure

We perform a χ^2 -fit, with 12 free parameters, to the following set of experimental data and conditions:

- $S_{01}(S_{2T2J})$ $\bar{K}N \rightarrow \bar{K}N$ and $\bar{K}N \rightarrow \pi\Sigma$ scattering amplitudes (real and imaginary parts) of Ref. [28], in the CM energy range of $1480 \text{ MeV} \leq \sqrt{s} \leq 1750 \text{ MeV}$

In this CM energy region, there are a total number of 56 data points (28 real and 28 imaginary parts) for each channel. The normalization used in Ref. [28] is different of that used here and their amplitudes, T_{ij}^{Go77} , are related to ours by:

$$T_{ij}^{\text{Go77}} = \text{sig}(i, j) |\vec{k}_i| \left[f_0^{\frac{1}{2}}(s) \right]_{j \leftarrow i}, \tag{15}$$

where $\text{sig}(i, j)$ is +1 for the elastic channel and -1 for the $\bar{K}N \rightarrow \pi\Sigma$ one. On the other hand, and because in Ref. [28] errors are not provided, we have taken for those amplitudes errors given by

$$\delta T_{ij}^{\text{Go77}} = \sqrt{(0.12 T_{ij}^{\text{Go77}})^2 + 0.05^2} \tag{16}$$

in the spirit of those used in Ref. [29].

- $S_{01} - \pi\Sigma$ mass spectrum [30], $1330 \text{ MeV} \leq \sqrt{s} \leq 1440 \text{ MeV}$: In this CM energy region, there are a total of thirteen 10 MeV bins and the experimental data are given in arbitrary units. To compare with data, taking into account the experimental acceptance of 10 MeV, we compute:

$$\frac{\Delta\sigma}{\Delta[M_{\pi\Sigma}(i)]} = C \int_{M_{\pi\Sigma}(i)-5\text{MeV}}^{M_{\pi\Sigma}(i)+5\text{MeV}} \left| \left[f_0^{\frac{1}{2}}(s=x^2) \right]_{2\leftarrow 2} \right|^2 |\vec{k}_2(s=x^2)| x^2 dx, \quad (17)$$

where C is an arbitrary global normalization factor³ and i denotes the bin with central CM energy $M_{\pi\Sigma}(i)$. Hence, there are only 12 independent data points. Finally, we take the error of the number of counts, N_i , of the bin i to be $1.61\sqrt{N_i}$ as in Ref. [31].

- The $K^-p \rightarrow \eta\Lambda$ total cross section of Ref. [32], $1662 \text{ MeV} \leq \sqrt{s} \leq 1684 \text{ MeV}$: We use the Crystal Ball Collaboration precise new total cross-section measurements (a total of 17 data points compiled in Table I of Ref. [32]) for the near-threshold reaction $K^-p \rightarrow \eta\Lambda$, which is dominated by the $\Lambda(1670)$ resonance. We assume, as in Ref. [32], that the p - and higher wave contributions do not contribute to the total cross-section.

Finally, we define the χ^2 , which is minimized, as

$$\chi^2/N_{\text{tot}} = \frac{1}{N} \sum_{\alpha=1}^N \frac{1}{n_{\alpha}} \sum_{j=1}^{n_{\alpha}} \left(\frac{x_j^{(\alpha)th} - x_j^{(\alpha)}}{\sigma_j^{(\alpha)}} \right)^2, \quad (18)$$

where $N = 4$ stands for the four sets of data used and discussed above⁴ and $x_j^{(\alpha)th}$ denotes our model result for the data point $x_j^{(\alpha)}$. Finally n_{α} takes the values 56, 56, 12 and 17, and $N_{\text{tot}} = \sum_{\alpha=1}^N n_{\alpha}$ is the total number of data points. With such a definition, acceptable best fits should provide values of χ^2/N_{tot} around one.

Though we have considered four coupled channels, three-body channels, for instance the $\pi\pi\Sigma$ one, are not explicitly considered, as it has been also assumed previously in Refs. [18] and [32].

3.2 Results of the best χ^2 fit

The model presented up to now has initially twelve free parameters (Eq. (12)), which have to be determined from data. This is a cumbersome task because there are many mathematical minima which are not physically admissible. For instance, in some cases one finds fits to data with spurious poles in the first Riemann Sheet which strongly influence the scattering region and hence violate causality. Any fit embodying these singularities is physically inadmissible and should be rejected. This is an important issue, which should always be considered in any analysis. We will further elaborate on this point in the Appendix B.

Furthermore, even if one is reasonably convinced that a physically acceptable minimum has been found, there are strong correlations between the fitting parameters, which have to be carefully evaluated and, if possible, understood. Our best results come from a minimum for which the pairs (J_i, Δ_{B_i}) with $i = \bar{K}N, \pi\Sigma, \eta\Lambda, K\Xi$ and $B_i = N, \Sigma, \Lambda, \Xi$ are totally correlated (correlation factors bigger than 0.99) which leads to an almost singular correlation matrix reflecting the fact that

³We fix it by setting the area of our theoretical spectrum, $\sum_i \frac{\Delta\sigma}{\Delta[M_{\pi\Sigma}(i)]}$, to the total number of experimental counts $\sum_i N_i$.

⁴From the first item above and to define the χ^2 , we consider two separated sets: $\bar{K}N \rightarrow \bar{K}N$ and $\bar{K}N \rightarrow \pi\Sigma$.

there exists, in very good approximation, a linear relation between the J_i and Δ_{B_i} parameters⁵. Thus, we have fixed Δ_{B_i} to some specific values in the neighborhood of the minimum, given in Appendix A, and have studied the correlation matrix for the remaining eight parameters. Yet, we find a strong correlation (0.99) between $J_{K\Xi}$ and Δ_K and we proceed as above, i.e., we fix Δ_K and evaluate the correlation matrix and variances for the remaining seven parameters. Thus, at the end of the day we have only seven independent best fit parameters. The best fit parameters, their variances and the correlation matrix are compiled in Appendix A.

In Figs. (2-4) we compare the results of our best fit with the experimental data. The overall description is remarkably good, both at low energies and the higher end of the considered energy region. Besides, as we will see, the description of the $\Lambda(1405)$ and $\Lambda(1670)$ features is also quite good. Thus, our scheme leads to a much better description of the data than the approach of Ref. [18], as it was also the case in the strangeness $S = 0$ sector ([23] versus [19]).

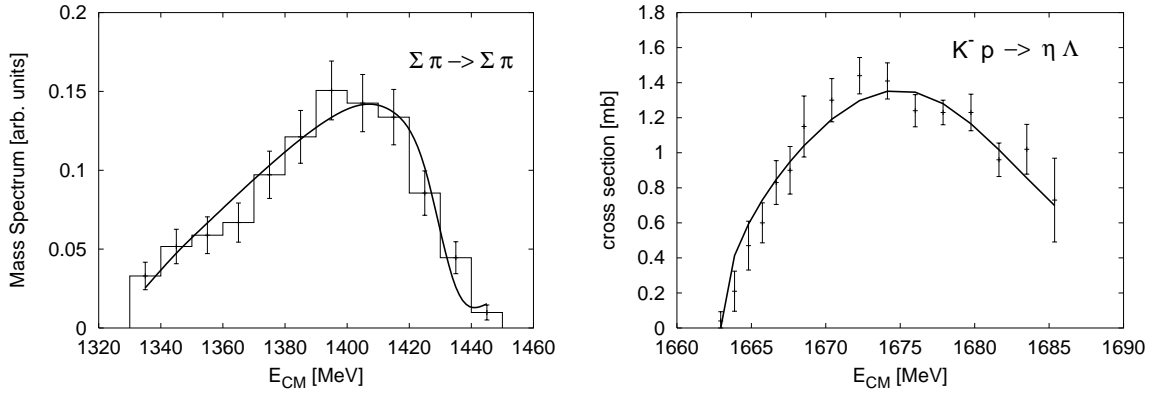


Figure 2: Solid lines: Results of our calculation. Experimental data for $\pi\Sigma \rightarrow \pi\Sigma$ and $K^-p \rightarrow \eta\Lambda$ are from Refs. [30] and [32], respectively

For the elastic $\bar{K}N \rightarrow \bar{K}N$ scattering length we get

$$a_{\bar{K}N} \equiv \left[f_0^{\frac{1}{2}}(s = (m_K + M_N)^2) \right]_{\bar{K}N \leftarrow \bar{K}N} = (-1.20 \pm 0.09 + i 1.29 \pm 0.09) \text{ fm} \quad (19)$$

where the error is statistical and it has been obtained from the covariance matrix given in the Appendix A, taking into account the existing statistical correlations, through a Monte-Carlo simulation. This value should be compared both to the experimental one $(-1.71 + i 0.68) \text{ fm}$ of Ref. [26] and to the LSE approach of Ref. [17] $(-2.24 + i 1.94) \text{ fm}$. Unfortunately, the previous works do not provide error estimates, so one cannot decide on the compatibility of results.

3.3 Second Riemann Sheet: poles and resonances.

In this section we are interested in describing masses and widths of the S_{01} - resonances in the $S = -1$ channel. Since causality imposes the absence of poles in the $t(s)$ matrix in the physical

⁵In Ref. [23] the static limit (infinitely heavy baryons) is discussed, and it is shown (Eq. (D9)) that there exists a linear relation between J_i and Δ_{B_i} if, as is the case here, Δ_{m_i} , $i = \bar{K}, \pi, \eta, K$ is small when compared to Δ_{B_i} .

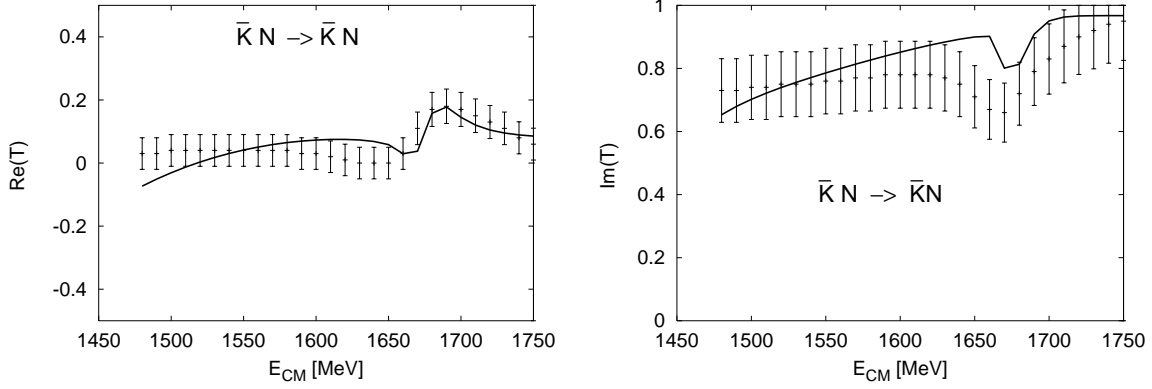


Figure 3: The real (left panel) and imaginary (right panel) parts of the s -wave T -matrix, with normalization specified in Eq. (16), for elastic $\bar{K}N \rightarrow \bar{K}N$ process in the $I = 0$ isospin channel as functions of the CM energy. The solid line is the result of our calculation, and the experimental data are taken from the analysis of Ref. [28] with the errors stated in the main text.

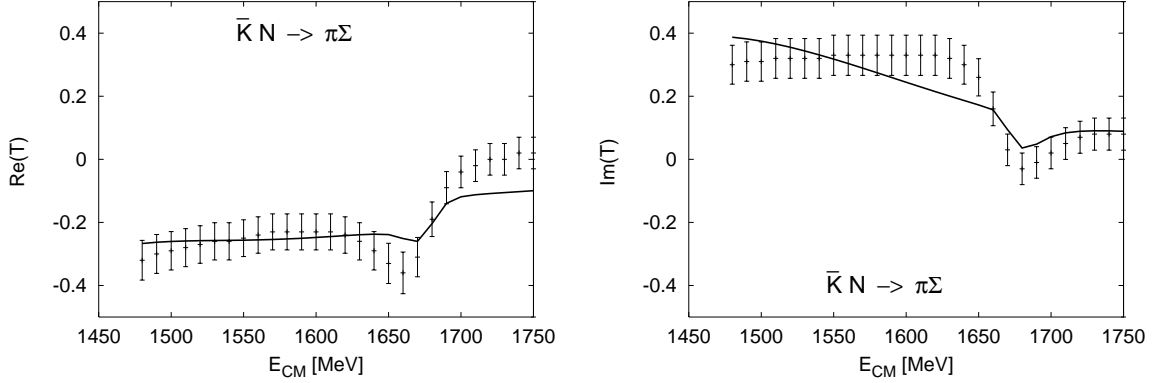


Figure 4: Same as in Fig. 3 for the inelastic channel $\bar{K}N \rightarrow \pi\Sigma$.

Sheet [36], one should search for complex poles in unphysical ones. Among all of them, those *closest* to the physical Sheet and hence to the scattering line are the most relevant ones. We define the second Riemann Sheet in the relevant fourth quadrant as that which is obtained by continuity across each of the four unitarity cuts (see a detailed discussion in a similar context in Ref. [23]). Physical resonances appear in the second Riemann Sheet of all matrix elements of $t(s)$, defined in Eq. (11), in the coupled channel space, differing only on the value of the residue at the pole. The residue determines the coupling of the resonances to the given channel. In Fig. 5 we show the absolute value of the $\eta\Lambda \rightarrow \eta\Lambda$ element of the t matrix. We choose this channel because all found poles have a sizeable coupling to it. Both the fourth quadrant of the second Riemann Sheet and the first quadrant of the first (physical) Riemann Sheet are shown. The physical scattering takes place in the scattering line in the plot (upper lip of unitarity cut of the first Riemann Sheet). We find three poles in the second Riemann Sheet which positions are ($s = M_R^2 - iM_R\Gamma_R$):

$$\text{First Pole : } M_R = 1368 \pm 12 \quad \Gamma_R = 250 \pm 23 \quad (20)$$

$$\text{Second Pole : } M_R = 1443 \pm 3 \quad \Gamma_R = 50 \pm 7 \quad (21)$$

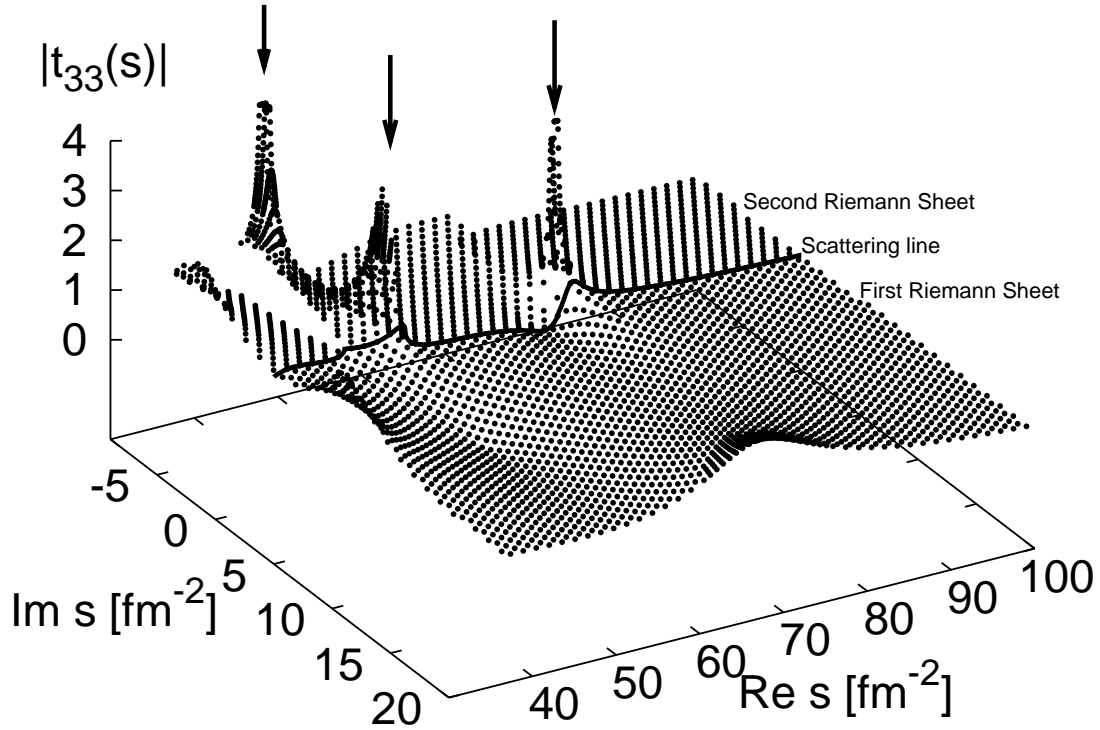


Figure 5: Modulus of the $\eta\Lambda \rightarrow \eta\Lambda$ element of the scattering amplitude $t(s)$ [fm], defined in Eq. (11), analytically extended to the first and fourth quadrants of the s -complex plane. The solid line is the scattering line, $s = x + i 0^+$, $x \in \mathbb{R}$, from the first threshold, $(m_\pi + M_\Sigma)^2$, on. The first (second) Riemann Sheet is depicted in the first (fourth) quadrant of the s complex plane. Three poles appear in the second Riemann Sheet, which are connected with the $\Lambda(1405)$ and $\Lambda(1670)$ resonances, see discussion in the main text. Besides unphysical poles show up in the physical Sheet out of the real axis, but they do not influence the scattering line as can be seen in the plot.

$$\text{Third Pole : } M_R = 1677.5 \pm 0.8 \quad \Gamma_R = 29.2 \pm 1.4 \quad (22)$$

where all units are given in MeV and errors have been transported from those in the best fit parameters (Eq. (40)), taking into account the existing statistical correlations through a Monte-Carlo simulation.

These poles are related to the two S_{01} resonances $\Lambda(1405)$ and $\Lambda(1670)$ which appear up to this range of energy in the PDG (Ref. [37]). The third pole above can be clearly identified to the $\Lambda(1670)$ which is located at

$$\begin{aligned} \Lambda(1670) : \quad M_R &= 1670 \pm 10 & \Gamma_R &= 35^{+15}_{-10} & \text{Ref. [37]} \\ M_R &= 1673 \pm 2 & \Gamma_R &= 23 \pm 6 & \text{Ref. [33]} \end{aligned} \quad (23)$$

where again units are in MeV. The agreement of our predictions and the experimental data is satisfactory and better than the previous theoretical LSE approach of Ref. [18]. Let us look at the $\Lambda(1405)$ resonance, which nature is under much discussion [34, 35]. Following the PDG it is placed at (in MeV)

$$\Lambda(1405) : \quad M_R = 1406.5 \pm 4.0 \quad \Gamma_R = 50 \pm 2 \quad \text{Ref. [37]} \quad (24)$$

Our amplitudes have two poles in the region of 1400 MeV, Eqs. (20) and (21). The features of the second one are in agreement with the previous results of Refs. [17, 18] and though the width compares well with the experiment, the mass is shifted to higher values. Besides, we should note that the pole quoted in Eq. (20) is very broad and can not be identified with any of the experimentally established resonances. This pole is also present in the LSE model of Refs. [17, 18], as it was pointed out in Ref. [38], though the mass position there is similar ($M_R = 1390$ MeV), the width is about a factor two narrower ($\Gamma_R = 132$ MeV) than ours. Our understanding is that this broad resonance does not influence strongly the scattering line. However, the $\pi\Sigma$ mass spectrum peaks around 1405 MeV in the experimental data and also in our approach as can be seen in Fig. 2. This is a clear indication of a sizeable non resonant contribution on top of our 1443 MeV pole.

On the other hand, there are unphysical poles in the physical (first) Riemann Sheet. These unphysical poles appear because we have truncated the iterated potential to solve the BSE. The two of them closer to the scattering line are located at $(s = M^2 + iM\Gamma)$ with $M \approx 1166$, $\Gamma \approx \pm 200$ MeV and $M \approx 1616$, $\Gamma \approx 631$ MeV. The tails of both poles can be seen in Fig. 5 and they do not influence the scattering line. In Appendix B, we will show the results from a fit which, at first sight, are even in a better agreement with the experimental data (Subsect. 3.1) than those presented up to now. However this apparent improvement is achieved because the unphysical poles get closer to the real s axis and they affect, in a substantial manner, the scattering amplitudes. Hence, we discard this minimum, and we would like to note that it is important to observe the positions and influence of the unphysical poles when deciding the goodness of a phenomenological description of data.

Finally, we have also analyzed the nature of resonances on the light of the well known Breit-Wigner parameterization for coupled channels and real s (See e.g. Ref. [39] and references therein),

$$t_{ij}^{\text{BW}}(s) = -\frac{\delta_{ij}}{2i\rho_i} [e^{2i\delta_i} - 1] + \frac{e^{i(\delta_i+\delta_j)} M_R \sqrt{\Gamma_i^{\text{BW}} \Gamma_j^{\text{BW}}}}{\sqrt{\rho_i \rho_j} [s - M_R^2 + iM_R \Gamma_R]} \quad (25)$$

for which the background is assumed to be diagonal in coupled channel space and the relative phase of the resonance to the background and the sum partial decay widths, $\sum_i \Gamma_i^{\text{BW}} = \Gamma_R$,

are chosen in such a way that $t_{ij}^{\text{BW}}(s)$ exactly fulfills unitarity on the real axis. Here, ρ_i is a kinematic factor defined by the second line of Eq. (31) below. The branching ratio is then defined as $B_i^{\text{BW}} = \Gamma_i^{\text{BW}}/\Gamma_R$. Subtracting the resonance contribution, Eq. (26), to the total amplitude we have found that for our $\Lambda(1670)$ the background is not a diagonal matrix, since for our t_{ij} -matrix we get $2\sum_{i<j} |t_{ij} - t_{ij}^{\text{RBW}}|^2 \approx \sum_i |t_{ii} - t_{ii}^{\text{RBW}}|^2$ for $s \rightarrow M_R^2$, with t_{ij}^{RBW} the second term in Eq. (25). In addition, the BW parameterization suggests a relation between the residue at the pole and the imaginary part of the pole. This relation is only true in the sharp resonance approximation, $\Gamma_i^{\text{BW}} \ll p_i$ with p_i the CM momentum of the decaying state. We have also checked that for our problem this is not the case. Actually, with such a definition we find that $\sum_i \Gamma_i^{\text{BW}} \approx 0.8\Gamma_R$ for the $\Lambda(1670)$. This is a simple consequence of the incorrect assumption made by Eq. (25).

3.4 Branching ratios and couplings of the resonances to different final states.

Before going further we would like to make some critical remarks regarding both the comparison between “theory” and “experiment”. Our BSE solution has a very specific energy dependence which, as we have seen in Subsect. 3.2, is able to fit numerically experimental data or rather a partial wave analysis with a given energy dependence. Obviously, both functional forms are not identical, and it is also fair to say that both incorporate their own biases. There is no reason to expect that they are numerically alike also in the complex plane⁶. Under these conditions, some parameters, like branching ratios, have a different meaning, since the extrapolation of the resonant contribution to the real s-axis is ambiguous. Actually, the ambiguity is enhanced as the resonance becomes wider and as a consequence the definition of a branching ratio becomes model dependent. We explain below our definition of branching ratios and how they are extracted from our amplitude.

Let us consider $s_R = M_R^2 - i M_R \Gamma_R$ a pole in the second Riemann Sheet of the coupled channel scattering matrix $t(s)$. Then, around the pole, it can be approximated by

$$[t(s)]_{ij} \approx 2M_R \frac{g_{ij}}{s - s_R}, \quad (26)$$

where g_{ij} is the residue matrix. Since t is a complex symmetric matrix (due to time reversal invariance), g is also complex symmetric and its rank is one to ensure that $s = s_R$ is a pole of order one of the $\det[t(s)]$. In this way a non-degenerate resonant state is being described⁷. Under

⁶A good example of this fact is provided by our best fit results of Subsect. 3.2 and the physically inadmissible results of Appendix B; they look very much the same on the scattering line although the analytic structure is rather different.

⁷This can be seen as follows. Using a matrix notation, the BSE reads $t(s) = V + V G_0(s) t(s)$ and it is solved by $t(s) = V(1 - G_0(s)V)^{-1}$, with the obvious identifications for V and G_0 . A pole, at $s = s_R$, in $\det[t(s)]$ is produced by a zero of $\det[1 - G_0(s)V]$. This last condition ensures that the homogeneous (quasi)bound state Bethe-Salpeter equation

$$(-G_0(s)^{-1} + V)\Psi = 0 \quad (27)$$

has a non trivial solution for $s = s_R$. Indeed, all solutions, Ψ , of the above equation are linear combination of the null eigenvectors of the $(1 - G_0(s_R)V)$ matrix and describe the dynamics of the existing states (resonances) at $s = s_R$. For a non-degenerate resonance (which we have checked it is indeed the case), the zero eigenspace should have dimension one. Whence for the case of four coupled channels, the rank of the matrix $(1 - G_0(s_R)V)$ is three and therefore $\det[1 - G_0(s)V]$ should have a single zero at $s = s_R$.

these conditions, g_{ij} turns out to be factorizable⁸,

$$g_{ij} = g_i g_j. \quad (28)$$

The above matrix, g_{ij} , has only one non-zero eigenvalue, $g_1^2 + g_2^2 + g_3^2 + g_4^2$, with g_i the associated eigenvector. The vector g_i determines the coupling of the resonance to the different final states, which are well and unambiguously defined even if the corresponding channels are closed in the decay of the resonance. In Table 1 we give the complex vectors g_i for the three resonances described in Subsect. 3.3. Unfortunately, the PDG does not provide this kind of information and, instead, branching ratios are given. To extract meaningful branching ratios from our calculation, we have to extrapolate the resonant contribution of the scattering amplitude to the s real axis, which is the only experimentally accessible. In addition, the picture of a resonance as a quantum mechanical decaying state, requires a probabilistic description. Thus, we isolate the resonant contribution to the S -matrix⁹ for $s = M_R^2$

$$\begin{aligned} S_{ij}^{\text{resonant}}(s = M_R^2) &= -2i \, 2M_R \sqrt{\rho_i^R} \frac{g_i g_j}{M_R^2 - s_R} \sqrt{\rho_j^R} \\ \rho_i(s) &= \Theta(s - s_{th}^i) \frac{|\vec{k}_i(s)|}{8\pi\sqrt{s}} \left(\sqrt{M_i^2 + \vec{k}_i^2} + M_i \right) \\ \rho_i^R &= \rho_i(s = M_R^2) \end{aligned} \quad (31)$$

with s_{th}^i the threshold of the baryon-meson channel i . This definition embodies a sensible kinematic suppression compatible with Cutkosky's rules and the s-wave nature of the resonance. Defining

$$b_i = g_i \sqrt{\frac{2\rho_i^R}{\Gamma_R}} \quad (32)$$

we find

$$S_{ij}^{\text{resonant}}(s = M_R^2) = -2i \, M_R \Gamma_R \frac{b_i b_j}{M_R^2 - s_R} \quad (33)$$

and taking into account that the matrix $b_{ij} = b_i b_j$ has rank 1 and that b_i (or any vector proportional to it) is the only eigenvector of S^{resonant} with a non zero eigenvalue, the resonant state at $s = M_R^2$ will be given by

$$|R\rangle \propto \sum_i b_i |i\rangle \quad (34)$$

⁸The symmetric complex matrix g can be diagonalized by a complex orthogonal transformation, U , as $g = U^T d U$, being only one element of the diagonal matrix d different of zero. If we take this element to be the d_{11} , we have $g_{ij} = (U^T)_{i1} d_{11} U_{1j} = d_{11} U_{1i} U_{1j}$.

⁹The S -matrix is related to the t matrix, in our convention, by:

$$S_{ij}(s) = \delta_{ij} - 2i \sqrt{\rho_i(s)} t_{ij}(s) \sqrt{\rho_j(s)} \quad (29)$$

and probability conservation ($S^\dagger S = S S^\dagger = 1$) holds since t fulfills coupled channel unitarity:

$$t_{ij}^*(s) - t_{ij}(s) = 2i \sum_k t_{ik}^*(s) \rho_k(s) t_{kj}(s). \quad (30)$$

| Resonance | $g_{\bar{K}N}$ | | $g_{\pi\Sigma}$ | | $g_{\eta\Lambda}$ | | $g_{K\Xi}$ | |
|----------------------------|----------------|----------|-----------------|----------|-------------------|----------|------------|------------|
| | $ g $ | ϕ | $ g $ | ϕ | $ g $ | ϕ | $ g $ | ϕ |
| $M_R = 1368 \text{ MeV}$ | 3.9(1) | -0.59(5) | 3.65(8) | -0.73(3) | 1.7(2) | 3.0(2) | 0.29(7) | 1.14(13) |
| $M_R = 1443 \text{ MeV}$ | 3.3(2) | 0.72(7) | 2.14(16) | 1.10(8) | 2.2(1) | -2.66(3) | 0.23(1) | -0.008(57) |
| $M_R = 1677.5 \text{ MeV}$ | 0.39(2) | -1.29(4) | 0.20(1) | 0.77(5) | 1.22(3) | 2.69(2) | 1.64(1) | -0.13(1) |

Table 1: Dimensionless complex couplings, $g_i = |g_i| e^{i\phi_i}$, defined in Eqs. (26-28), for all channels $i = \bar{K}N$, $\pi\Sigma$, $\eta\Lambda$, $K\Xi$, and for the three poles (resonances) quoted in Eqs. (20–22). The phases are in radian units. Errors are purely statistical and affect the last significant digit.

where $|i\rangle$ stands for the meson-baryon states used to build the coupled channel space. Finally, the branching ratio B_i will be given by the probability of finding $|R\rangle$ in the state $|i\rangle$

$$B_i = \frac{|b_i|^2}{\sum_j |b_j|^2} \quad (35)$$

which by definition fulfills $\sum_i B_i = 1$. The partial decay width may then be defined as $\Gamma_i = B_i \Gamma_R$, and obviously $\sum_i \Gamma_i = \Gamma_R$. For the $\Lambda(1670)$ we obtain the following branching ratios with the above prescription:

$$B_{\bar{K}N} = 0.24 \pm 0.01, \quad B_{\pi\Sigma} = 0.08 \pm 0.01, \quad B_{\eta\Lambda} = 0.68 \pm 0.01 \quad (36)$$

The last two values are not in agreement with the values quoted in the PDG [37] ($B_{\bar{K}N} = 0.25 \pm 0.05$, $B_{\pi\Sigma} = 0.40 \pm 0.15$, $B_{\eta\Lambda} = 0.17 \pm 0.07$) and in Ref. [33] ($B_{\bar{K}N} = 0.37 \pm 0.07$, $B_{\pi\Sigma} = 0.39 \pm 0.08$, $B_{\eta\Lambda} = 0.16 \pm 0.06$, $B_{\pi\Sigma(1385)} = 0.08 \pm 0.06$).

To finish this subsection, we would like to point out that in the present context the concept of branching ratio is subtle and it might be ambiguous, both from the theoretical and experimental sides. From the experimental point of view the difficulty arises from the impossibility of preparing a pure short-lived resonant state strongly coupled to a continuum and therefore the impossibility of disentangle events coming from the formation of the resonance from those produced through non-resonant processes. From the theoretical point of view the ambiguity comes when defining $S^{\text{resonant}}(s = M_R^2)$ in Eq. (31). For instance at the pole $s = s_R$ one could have

$$[t(s)]_{ij} \approx 2M_R \frac{\beta_i(s)}{\beta_i(s_R)} \frac{g_{ij}}{s - s_R} \frac{\beta_j(s)}{\beta_j(s_R)}, \quad (37)$$

instead of the expression assumed in Eq. (26), being $\beta_i(s)$ an arbitrary, analytical around s_R , complex function. In these circumstances the matrix $S_{ij}^{\text{resonant}}(s = M_R^2)$ would be different from that given in Eq. (31) by a factor $\frac{\beta_i(M_R^2)}{\beta_i(s_R)} \frac{\beta_j(M_R^2)}{\beta_j(s_R)}$ and one would get a new vector \tilde{b}_i which in terms of the vector b_i , defined in Eq. (32), reads:

$$\tilde{b}_i = \frac{\beta_i(M_R^2)}{\beta_i(s_R)} b_i \quad (38)$$

leading to, in principle, different branching ratios. The trouble comes from the extrapolation from s_R to the real axis which is not unique.

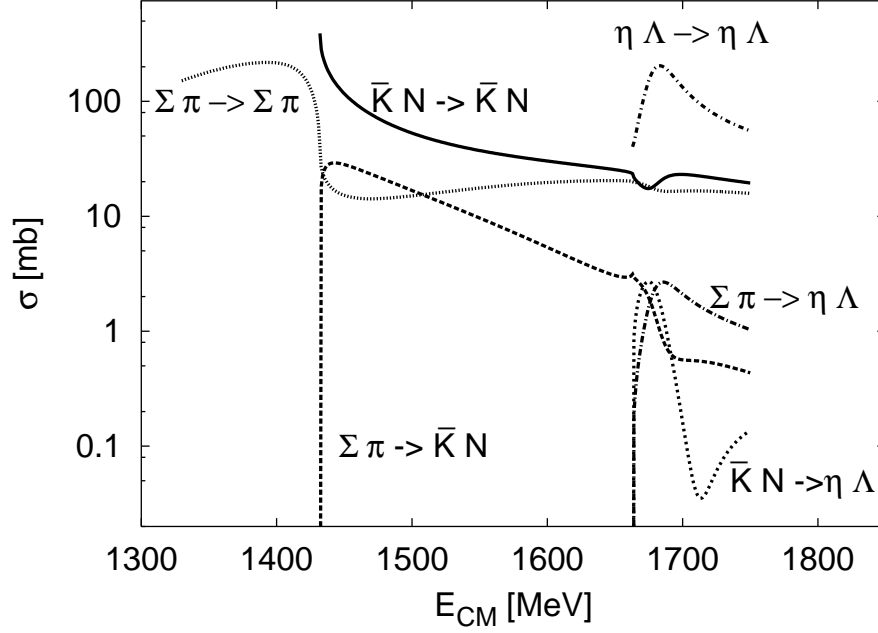


Figure 6: $I = 0$ meson-baryon s -wave cross sections for different channels.

The usual assumption is that the $\beta_i(s)$ functions are smooth and they do not change much from $s = s_R$ to $s = M_R^2$, and more important, that the change does not depend significantly on the channel i . However, this is not always true, for example, if one were dealing with a p -wave resonance the function $\beta_i(s)$ would at least include the CM meson baryon momentum. If there is a channel which gets open close and above to $s = M_R^2$, then the CM momentum would lead to a suppression of the branching ratio to this channel.

3.5 Predictions for other processes

In Fig. 6 we show some of our predictions for s -wave $I = 0$ cross sections for some elastic and inelastic channels. For most of them there are no data. The effect of the $\Lambda(1405)$ resonance is clearly visible in the $\Sigma\pi \rightarrow \Sigma\pi$ and $\Sigma\pi \rightarrow \bar{K}N$ and $\bar{K}N \rightarrow \bar{K}N$ cross sections. On the other hand, the elastic $\eta\Lambda$ cross section takes a very large value at threshold, which corresponds to a typical low energy resonance behavior triggered by the $\Lambda(1670)$ resonance. This is in contrast to any expectation based in the Born approximation, since the corresponding potential in this channel vanishes (Eq. (9)). Our estimates for $\pi\Sigma$ and $\eta\Lambda$ scattering lengths (defined for the elastic channels similarly as in Eq. (19)) are

$$\begin{aligned} a_{\pi\Sigma} &= 1.10 \pm 0.06 \text{ fm} \\ a_{\eta\Lambda} &= (0.50 \pm 0.05) + i(0.27 \pm 0.01) \text{ fm} \end{aligned} \quad (39)$$

respectively.

4 Conclusions

In this paper we have extended the Bethe-Salpeter formalism developed in Ref. [23] to study s -wave and $I = 0$ meson-baryon scattering up to 1.75 GeV in the strangeness $S = -1$ sector. We work on a four dimensional two body channel space and the kernel of the BSE takes into account CS constraints as deduced from the corresponding effective Lagrangian. The obtained t matrix manifestly complies with coupled channel unitarity and the undetermined low-energy constants of the model have been fitted to data. The available direct experimental information is limited to the $\pi\Sigma \rightarrow \pi\Sigma$ mass spectrum, and the $K^-p \rightarrow \Lambda\eta$ total cross section, for which errors are provided, and to $\bar{K}N \rightarrow \bar{K}N$ and $\bar{K}N \rightarrow \pi\Sigma$ scattering amplitudes of a partial wave analysis, for which errors are guessed. Taking this into account, the agreement with experiment is satisfactory. Besides, some predictions for other cross sections, not yet measured, have been also given. A careful and detailed statistical study has been carried out, showing that only seven parameters (LEC's) out of the starting twelve are really independent. Thus, though our model has some more free parameters than those required in Ref. [18], the description of data achieved in our approach is superior to that of Ref. [18]. A similar situation was already found also in the strangeness $S = 0$ sector [23]. According to previous experience, the reduction of parameters is partly due to the constraint of a well defined heavy baryon limit [23]. Likewise, crossing symmetry is expected to shed more light on the number of independent LEC's. As we have argued, matching to HBChPT calculations in the $S = -1$ and $I = 0$ sector would be the ideal way to map our LEC's into those stemming from an effective chiral Lagrangian, but it is already known [25] that the chiral expansion fails to reproduce the $\bar{K}N$ scattering length, due to the influence of the nearby subthreshold $\Lambda(1405)$ resonance. We believe these points deserve a deeper investigation.

We have undertaken a careful discussion on the analytical structure of the scattering matrix amplitude in the complex s -plane, which becomes mandatory in order to extract the features of the S_{01} resonances. We have searched for poles in the second Riemann Sheet and compared masses, widths and branching ratios to data. The agreement is also quite satisfactory. In the resonance region our unitary amplitude cannot be analyzed as a Breit-Wigner resonance due to a sizeably non-diagonal background in coupled channel space. This, in particular, prevents from a simple interpretation of branching ratios. Although residues at the resonance poles are well and unambiguously defined, the definition of branching ratios requires special considerations and provisos, due to an ambiguous extrapolation of the resonance contribution of the S-matrix from the pole to the scattering line. We have also illustrated that looking for a good description of experimentally accessible data is not sufficient and that, in some cases, it can be achieved at the expense of generating non-physically acceptable poles in the first Riemann Sheet, which influence on the scattering region is non-negligible. Thus, any fit to data should be supplemented by this additional requirement of not producing spurious singularities numerically relevant for the description of scattering processes.

Acknowledgments

We warmly thank E. Oset and A. Ramos for useful discussions. This research was supported by DGES under contracts BFM2000-1326 and PB98-1367 and by the Junta de Andalucia.

A Best fit results

The best fit ($\chi^2/N_{\text{tot}} = 0.93$) parameters are

$$\begin{aligned}
J_{\bar{K}N} &= -0.0186 \pm 0.0010 \\
J_{\pi\Sigma} &= 0.00796 \pm 0.00061 \\
J_{\eta\Lambda} &= 0.01264 \pm 0.00021 \\
J_{K\Xi} &= -0.11936 \pm 0.00018 \\
\bar{\Delta}_N \equiv \Delta_N/(m_{\bar{K}} + M_N)^2 &= 0.01355 \pm 0.00029 \\
\bar{\Delta}_\Sigma \equiv \Delta_\Sigma/(m_\pi + M_\Sigma)^2 &= -0.00325 \pm 0.00036 \\
\bar{\Delta}_\Lambda \equiv \Delta_\Lambda/(m_\eta + M_\Lambda)^2 &= -0.00262 \pm 0.00011
\end{aligned} \tag{40}$$

with fixed parameters

$$\begin{aligned}
\Delta_\Xi/(m_K + M_\Xi)^2 &= -0.0035 \\
\Delta_{\bar{K}}/(m_{\bar{K}} + M_N)^2 &= -0.034 \\
\Delta_\pi/(m_\pi + M_\Sigma)^2 &= 0.060 \\
\Delta_\eta/(m_\eta + M_\Lambda)^2 &= 0.049 \\
\Delta_K/(m_K + M_\Xi)^2 &= -0.26
\end{aligned} \tag{41}$$

as explained in the main text. We assume that the parameters of Eq. (40) are Gaussian correlated, this is justified because they come from a χ^2 -fit. To make any further statistical analysis of quantities derived from the parameters above, the corresponding covariance (v) and correlation (c) matrices are needed. These matrices are defined as usual

$$\begin{aligned}
v_{ij} &= \left[\left(\frac{1}{2} \frac{\partial \chi^2}{\partial b_i \partial b_j} \right)^{-1} \right]_{ij} \\
c_{ij} &= v_{ij} / \sqrt{v_{ii} v_{jj}},
\end{aligned} \tag{42}$$

being b_i any of the seven parameters J 's and Δ 's of Eq. (40). The errors, δb_i , quoted in Eq. (40) are obtained from the diagonal elements of the covariance matrix ($\delta b_i = \sqrt{v_{ii}}$). Finally our estimate for the correlation matrix reads:

$$\begin{pmatrix}
& J_{\bar{K}N} & J_{\pi\Sigma} & J_{\eta\Lambda} & J_{K\Xi} & \bar{\Delta}_N & \bar{\Delta}_\Sigma & \bar{\Delta}_\Lambda \\
J_{\bar{K}N} & 1.000 & & & & & & \\
J_{\pi\Sigma} & -0.236 & 1.000 & & & & & \\
J_{\eta\Lambda} & -0.909 & 0.442 & 1.000 & & & & \\
J_{K\Xi} & 0.569 & -0.479 & -0.530 & 1.000 & & & \\
\bar{\Delta}_N & -0.830 & 0.228 & 0.702 & -0.829 & 1.000 & & \\
\bar{\Delta}_\Sigma & 0.294 & 0.608 & -0.030 & 0.224 & -0.494 & 1.000 & \\
\bar{\Delta}_\Lambda & -0.158 & -0.501 & 0.087 & 0.613 & -0.336 & -0.051 & 1.000
\end{pmatrix} \tag{43}$$

Despite the correlations in the above matrix are at most in modulus of about 0.9, the matrix has got an eigenvalue quite close to zero (0.0025), which is a clear indication that one of the parameters might still be redundant.

B Non-physically acceptable fits to data

In Figs. (7-9) we present the results of a fit to the data, which we will show is not physically acceptable. The overall description of data is remarkably good. This fit gives $\chi^2/N_{\text{tot}} = 0.69$ to compare with the value of 0.93 of the best fit presented in the main text. However, when

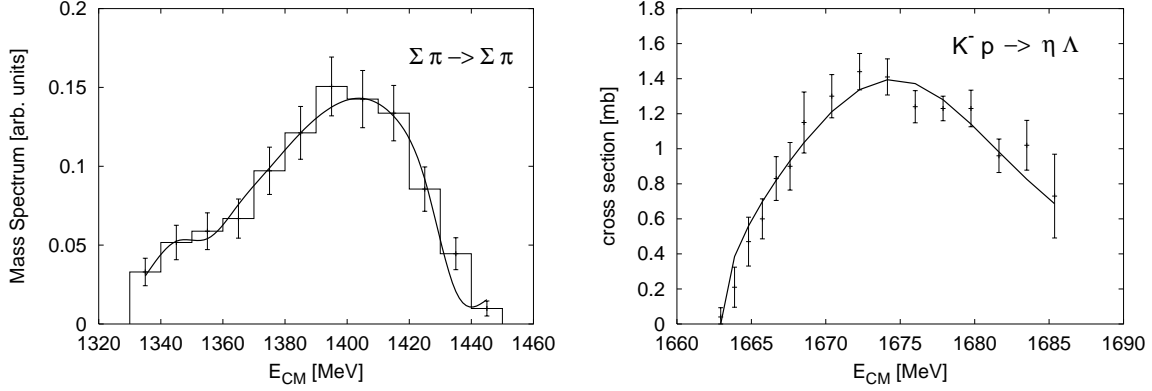


Figure 7: Same as in Fig. (2) for “the non physically acceptable fit” described in the Appendix B.

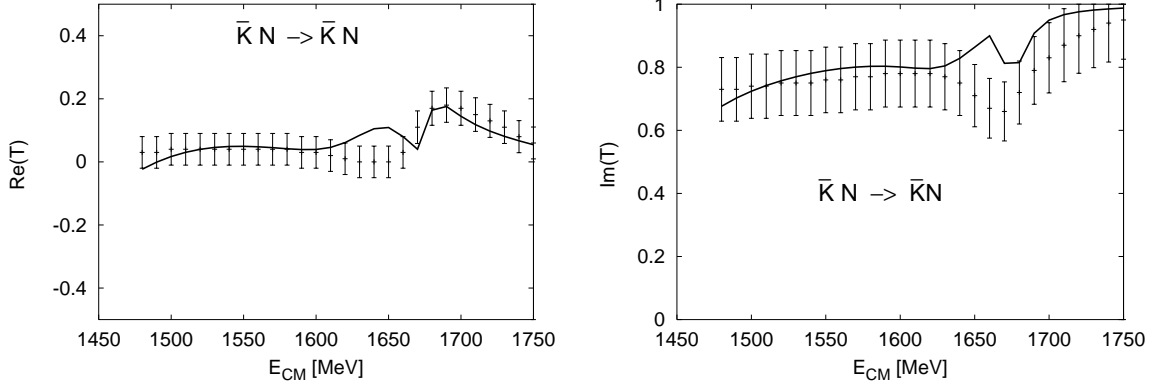


Figure 8: Same as in Fig. (3) for “the non physically acceptable fit” described in the Appendix B.

looking at the $t(s)$ matrix in the s -complex plane (Fig. (10)), one realizes that there exists a proliferation of poles, some of them unphysical and others with no experimental counterparts. In the first Riemann Sheet we find at least two poles. The first one is located at $s = M^2 - iM\Gamma$ with $M = 1606$ MeV and $\Gamma = 153$ MeV. This pole is close to the s real axis and produces visible effects on the scattering line not only for the $t_{\eta\Lambda \rightarrow \eta\Lambda}$ entry shown in the figure, but also for all $i \rightarrow j$ channels. Indeed, as we showed in Subsect. 3.3, our preferred fit has also a similar unphysical pole but significantly farther ($\Gamma = 631$ MeV) from the real axis, and therefore with a tiny influence on the physical scattering. Since causality imposes the absence of poles in the physical Sheet [36], the existence of such a pole affecting the scattering line invalidates the description (Figs. (7-9)) presented in this Appendix, despite of its quality. Besides in the first Sheet, there exists a pole

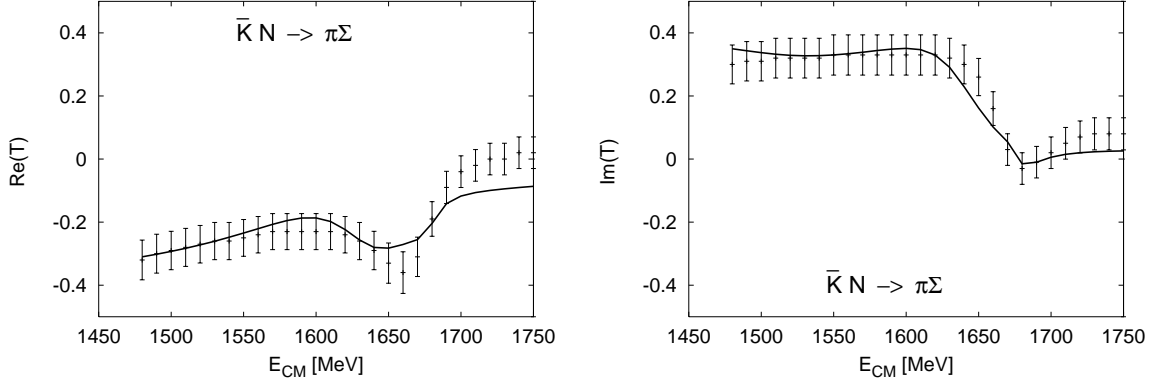


Figure 9: Same as in Fig. 8 for the inelastic channel $\bar{K}N \rightarrow \pi\Sigma$.

on the real axis ($\sqrt{s} = 1307$ MeV) and below the first threshold, which would correspond to a bound state, stable under strong interactions. Such a state has the same quantum numbers as the $\Lambda(1115)$ and it should show up in all reactions where the latter one is produced.

On the other hand, in the second Sheet there exist now four poles. Three of them are similar to those presented in Subsect. 3.3, though the one placed around 1370 MeV (Eq. (20)) is now almost a factor two narrower (it is located at $M_R = 1392$ MeV and $\Gamma_R = 120$ MeV). In addition there exists a new resonance $M_R = 1343$ MeV and $\Gamma_R = 0.18$ MeV which is responsible of the high peak at the beginning of the scattering line in Fig. 10 and of the existing bump between 1330 and 1360 MeV in the $\pi\Sigma$ mass spectrum of Fig. 7. As far as we know, there are no other independent indications of the existence of this extremely narrow resonance.

We have presented the results of this “non physically acceptable fit” to stress that, in order to be sure of having a good approach to the t matrix of a given physical system, one should *not only* look at the t matrix and related observables (cross sections, ...) at the physical scattering line (real s values), but one should *also* study its behavior on the s -complex plane, both in the second Riemann Sheet to find the resonances and in the first Riemann Sheet to be sure of avoiding pathological behaviors as the one illustrated in Fig. 10.

References

- [1] For a review see e.g. M. Arima, K. Masutani and T. Sato, Prog. Theor. Phys. Suppl. **137** (2000) 169.
- [2] A. Pich, Rep. Prog. Phys. **58** (1995) 563.
- [3] E. Jenkins and A. V. Manohar, Phys. Lett. **B 255** (1991) 558.
- [4] V. Bernard, N. Kaiser, J. Kambor and Ulf G. Meissner, Nucl. Phys. **B 388** (1992) 315.
- [5] M. Mojziz, Eur. Phys. J. **C 2** (1998) 181.
- [6] N. Fettes, Ulf-G. Meissner and S. Steininger; Nucl. Phys. **A 640** (1988) 199.
- [7] N. Fettes and Ulf. G. Meißner, Nucl. Phys. **A 676** (2000) 311.

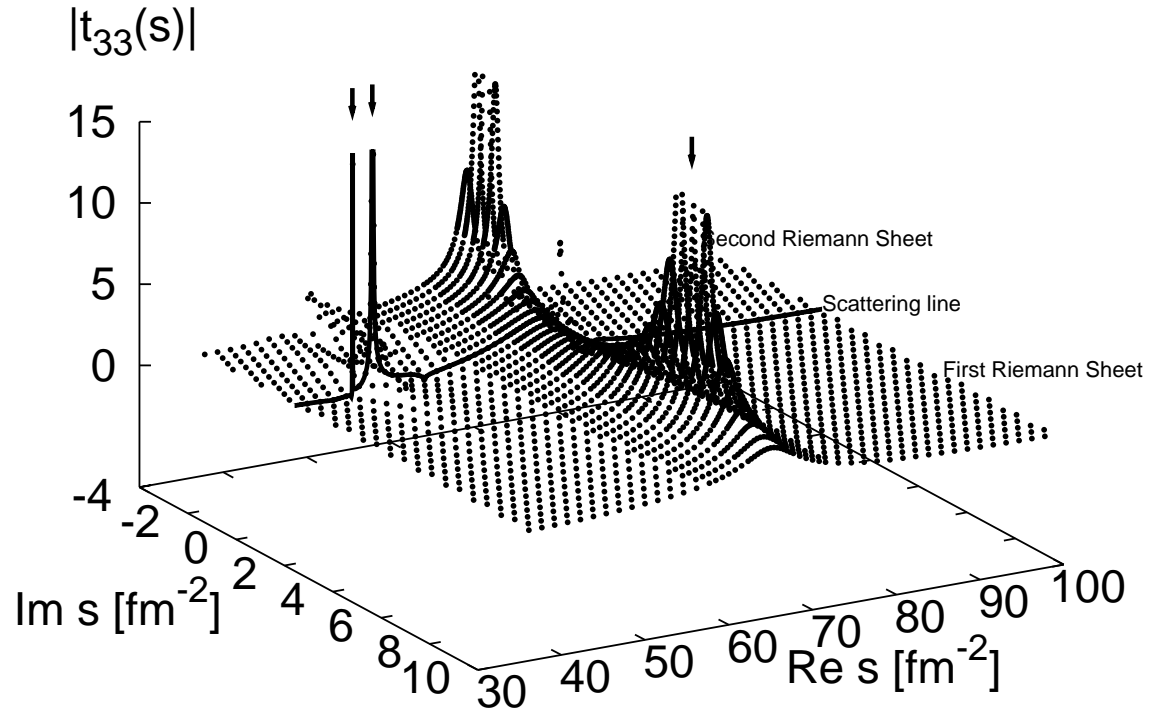


Figure 10: Same as in Fig. (5) for a the non physically acceptable fit to data described in the AppendixB.

- [8] T. Becher and H. Leutwyler, Eur. Phys. Jour. **C 9** (1999) 643.
- [9] T. Becher and H. Leutwyler, JHEP **0106** (2001) 017
- [10] J.R. Peláez and A. Gómez Nicola, Phys. Rev. **D 62** (2000) 017502.
- [11] J. Nieves and E. Ruiz Arriola, *hep-ph/0001013*; Gómez Nicola, J. Nieves, J.R. Peláez and E. Ruiz Arriola, Phys. Lett. **B 486** (2000) 77.
- [12] J. Nieves and E. Ruiz Arriola, Phys. Rev. **D 63**, (2001) 076001 .
- [13] J. A. Oller and Ulf. G. Meißner, Physl. Lett. **500** (2001) 263.
- [14] N. Kaiser, P.B. Siegel and W. Weise, Nucl. Phys. **A 594** (1995) 325;
- [15] N. Kaiser, P.B. Siegel and W. Weise, Phys. Lett. **B 362** (1995) 23.
- [16] J. Caro Ramon, N. Kaiser, S. Wetzel and W. Weise, Nucl. Phys. **A 672** (2000) 249.
- [17] E. Oset and A. Ramos, Nucl. Phys. **A 635** (1998) 99.
- [18] E. Oset, A. Ramos and C. Bennhold, Phys. Lett. **B 527** (2002) 99; Erratum, *ibid.* **B 530** (2002)260.
- [19] J. C. Nacher, A. Parreño, E. Oset, A. Ramos, A. Hosaka and M. Oka, Nucl. Phys. **A 678** (2000) 187.
- [20] T. Inoue, E. Oset and M.J. Vicente-Vacas, Phys. Rev. **C 65** (2002)035204.
- [21] C. Garcia-Recio, J. Nieves, E. Ruiz Arriola and M. Vicente Vacas, to appear in the *Proceedings of Conference on Quarks and Nuclear Physics (QNP 2002)* (Julich, Germany, 2002) nucl-th/0209053.
- [22] C. Garcia-Recio, J. Nieves, E. Ruiz Arriola and M. Vicente Vacas, to appear in the *Proceedings of PANIC02* (Osaka, Japan, 2002).
- [23] J. Nieves and E. Ruiz Arriola, Phys. Rev. **D 64** (2001) 116008.
- [24] M. F. M. Lutz and E. E. Kolomeitsev, Nucl. Phys. **A 700** (2002) 193.
- [25] N. Kaiser, Phys. Rev. **C 64** (2001) 045204.
- [26] A.D. Martin, Nucl. Phys. **B 179** (1981) 33.
- [27] J. Nieves and E. Ruiz Arriola, Phys. Lett. **B 455** (1999) 30; *ibidem* Nucl. Phys. **A 679** (2000) 57.
- [28] G.P. Gopal *et al.*, Nucl. Phys. **B 119** (1977) 362.
- [29] M.Th. Keil, G. Penner and U. Mosel, Phys. Rev. **C 63** (2001) 045202.
- [30] R.J. Hemingway, Nucl Phys. **B 253** (1984) 742.
- [31] R.H. Dalitz and A. Deloff, J. Phys. G: Nucl. Part. Phys. **17** (1991) 289.

- [32] A. Starostin *et al.*, Phys. Rev. **C 64** (2001) 055205.
- [33] D.M. Manley *et al.*, Phys. Rev. Let. **88** (2002) 012002-1.
- [34] R. H. Dalitz, Eur. Phys. J. **C 3** (1998) 676.
- [35] M. Kimura, T. Miyakawa, A. Suzuki, M. Takayama, K. Tanaka and A. Hosaka, Phys. Rev. **C 62** (2000) 015206.
- [36] S. Mandelstam, Phys. Rev. **112** (1958) 1344.
- [37] K. Hagiwara *et al.*, Phys. Rev. **D 66** (2002) 010001.
- [38] D. Jido, A. Hosaka, J.C. Nacher, E. Oset and A. Ramos, Phys. Rev. **C 66** (2002) 025203.
- [39] A. M. Badalyan, L. P. Kok, M. L. Polykarpov and Yu. A. Simonov, Phys. Rep. **82** (1982) 31.